



Gill, M. S., Lemey, P., Bennett, S. N., Biek, R. and Suchard, M. A. (2016) Understanding past population dynamics: Bayesian coalescent-based modeling with covariates. *Systematic Biology*, 65(6), pp. 1041-1056. (doi: [10.1093/sysbio/syw050](https://doi.org/10.1093/sysbio/syw050))

This is the author's final accepted version.

There may be differences between this version and the published version. You are advised to consult the publisher's version if you wish to cite from it.

<http://eprints.gla.ac.uk/119885/>

Deposited on: 15 July 2016

Enlighten – Research publications by members of the University of Glasgow
<http://eprints.gla.ac.uk>

1

2 RH: Understanding Past Population Dynamics

3 **Understanding Past Population Dynamics: Bayesian**
4 **Coalescent-Based Modeling with Covariates**

5 MANDEV S. GILL¹, PHILIPPE LEMEY², SHANNON N. BENNETT³, ROMAN BIEK⁴

6 AND MARC A. SUCHARD^{5,6,7}

7 *¹Department of Statistics, Columbia University, New York, United States*

8 *²Department of Microbiology and Immunology, Rega Institute, KU Leuven, Leuven, Belgium*

9 *³Department of Microbiology, California Academy of Sciences, San Francisco, United States*

10 *⁴Boyd Orr Centre for Population and Ecosystem Health, Institute of Biodiversity, Animal Health*
11 *and Comparative Medicine, College of Medical, Veterinary and Life Sciences, University of*
12 *Glasgow, Glasgow, United Kingdom*

13 *⁵Department of Biomathematics, David Geffen School of Medicine at UCLA, University of*
14 *California, Los Angeles, United States*

15 *⁶Department of Human Genetics, David Geffen School of Medicine at UCLA, University of*
16 *California, Los Angeles, United States*

17 *⁷Department of Biostatistics, Jonathan and Karin Fielding School of Public Health, University of*
18 *California, Los Angeles, United States*

19 **Corresponding author:** Marc A. Suchard, Departments of Biostatistics,
20 Biomathematics, and Human Genetics, University of California, Los Angeles, 695 Charles
21 E. Young Dr., South, Los Angeles, CA 90095-7088, USA; E-mail: msuchard@ucla.edu

22 *Abstract.*— Effective population size characterizes the genetic variability in a population
23 and is a parameter of paramount importance in population genetics and evolutionary
24 biology. Kingman’s coalescent process enables inference of past population dynamics
25 directly from molecular sequence data, and researchers have developed a number of flexible
26 coalescent-based models for Bayesian nonparametric estimation of the effective population
27 size as a function of time. Major goals of demographic reconstruction include identifying
28 driving factors of effective population size, and understanding the association between the
29 effective population size and such factors. Building upon Bayesian nonparametric
30 coalescent-based approaches, we introduce a flexible framework that incorporates
31 time-varying covariates that exploit Gaussian Markov random fields to achieve temporal
32 smoothing of effective population size trajectories. To approximate the posterior
33 distribution, we adapt efficient Markov chain Monte Carlo algorithms designed for highly
34 structured Gaussian models. Incorporating covariates into the demographic inference
35 framework enables the modeling of associations between the effective population size and
36 covariates while accounting for uncertainty in population histories. Furthermore, it can
37 lead to more precise estimates of population dynamics. We apply our model to four
38 examples. We reconstruct the demographic history of raccoon rabies in North America and
39 find a significant association with the spatiotemporal spread of the outbreak. Next, we
40 examine the effective population size trajectory of the DENV-4 virus in Puerto Rico along
41 with viral isolate count data and find similar cyclic patterns. We compare the population
42 history of the HIV-1 CRF02_AG clade in Cameroon with HIV incidence and prevalence
43 data and find that the effective population size is more reflective of incidence rate. Finally,
44 we explore the hypothesis that the population dynamics of musk ox during the Late
45 Quaternary period were related to climate change.
46 (Keywords: Coalescent, Effective Population Size, Phylogenetics, Phylodynamics,
47 Population Genetics, Gaussian Markov Random Fields)

48 The effective population size is an abstract parameter of fundamental importance in
49 population genetics, evolutionary biology and infectious disease epidemiology. Wright
50 (1931) introduces the concept of effective population size as the size of an idealized
51 Fisher-Wright population that gains and loses genetic diversity at the same rate as the real
52 population under study. The Fisher-Wright model is a classic forward-time model of
53 reproduction that assumes random mating, no selection or migration, and non-overlapping
54 generations. Coalescent theory (Kingman 1982a,b) provides a probabilistic model for
55 generating genealogies relating samples of individuals arising from a Fisher-Wright model
56 of reproduction. Importantly, the coalescent elucidates the relationship between population
57 genetic parameters and ancestry. In particular, the dynamics of the effective population
58 size greatly inform the shapes of coalescent-generated genealogies. This opens the door for
59 the inverse problem of coalescent-based inference of effective population size trajectories
60 from gene genealogies.

61 While the coalescent was originally developed for constant-size populations,
62 extensions that accommodate a variable population size (Slatkin and Hudson 1991;
63 Griffiths and Tavaré 1994; Donnelly and Tavaré 1995) provide a basis for estimation of the
64 effective population size as a function of time (also called the demographic function). Early
65 approaches assumed simple parametric forms for the demographic function, such as
66 exponential or logistic growth, and provided maximum likelihood (Kuhner et al. 1998) or
67 Bayesian (Drummond et al. 2002) frameworks for estimating the parameters that
68 characterized the parametric forms. However, *a priori* parametric assumptions can be quite
69 restrictive, and finding an appropriate parametric form for a given demographic history can
70 be time consuming and computationally expensive. To remedy this, there has been
71 considerable development of nonparametric methods to infer past population dynamics.

72 Nonparametric coalescent-based models typically approximate the effective
73 population size as a piecewise constant or linear function. The methodology has evolved

74 from fast but noisy models based on method of moments estimators (Pybus et al. 2000;
75 Strimmer and Pybus 2001), to a number of flexible Bayesian approaches, including
76 multiple change-point models (Opgen-Rhein et al. 2005; Drummond et al. 2005; Heled and
77 Drummond 2008), and models that employ Gaussian process-based priors on the
78 population trajectory (Minin et al. 2008; Gill et al. 2013; Palacios and Minin 2013).
79 Extending the basic methodological framework to incorporate a number of key features,
80 including accounting for phylogenetic error (Drummond et al. 2005; Minin et al. 2008;
81 Heled and Drummond 2008; Gill et al. 2013), the ability to analyze heterochronous data
82 (Pybus et al. 2000; Drummond et al. 2005; Minin et al. 2008; Heled and Drummond 2008;
83 Gill et al. 2013; Palacios and Minin 2013), and simultaneous analysis of multilocus data
84 (Heled and Drummond 2008; Gill et al. 2013) has hastened progress.

85 In spite of all of these advances, there remains a need for further development of
86 population dynamics inference methodology. One promising avenue is introduction of
87 covariates into the inference framework. A central goal in demographic reconstruction is to
88 gain insights into the association between past population dynamics and external factors
89 (Ho and Shapiro 2011). For example, Lorenzen et al. (2011) combine demographic
90 reconstructions from ancient DNA with species distribution models and the human fossil
91 record to elucidate how climate and humans impacted the population dynamics of woolly
92 rhinoceros, woolly mammoth, wild horse, reindeer, bison and musk ox during the Late
93 Quaternary period. Lorenzen et al. (2011) show that changes in megafauna abundance are
94 idiosyncratic, with different species (and continental populations within species)
95 responding differently to the effects of climate change, human encroachment and habitat
96 redistribution. Lorenzen et al. (2011) identify climate change as the primary explanation
97 behind the extinction of Eurasian musk ox and woolly rhinoceros, point to a combination
98 of climatic and anthropogenic factors as the causes of wild horse and steppe bison decline,
99 and observe that reindeer remain largely unaffected by any such factors. Similarly, Stiller

100 et al. (2010) examine whether climatic changes were related to the extinction of the cave
101 bear, and Finlay et al. (2007) consider the impact of domestication on the population
102 expansion of bovine species. Comparison of external factors with past population dynamics
103 is also a popular approach in epidemiological studies to explore hypotheses about the
104 spread of viruses (Lemey et al. 2003; Faria et al. 2014).

105 In addition to the association between past population dynamics and potential
106 driving factors, it is of fundamental interest to assess the association between effective
107 population size and census population size (Crandall et al. 1999; Liu and Mittler 2008; Volz
108 et al. 2009; Palstra and Fraser 2012). For instance, Bazin et al. (2006) argue that in
109 animals, diversity of mitochondrial DNA (mtDNA) is not reflective of population size,
110 whereas allozyme diversity is. Atkinson et al. (2008) follow up by examining whether
111 mtDNA diversity is a reliable predictor of human population size. The authors compare
112 Bayesian Skyline (Drummond et al. 2005) effective population size reconstructions with
113 historical estimates of census population sizes and find concordance between the two
114 quantities in terms of relative regional population sizes.

115 Existing methods for population dynamics inference do not incorporate covariates
116 directly into the model, and associations between the effective population size and
117 potentially related factors are typically examined in post hoc fashions that ignore
118 uncertainty in demographic reconstructions. We propose to fill this void by including
119 external time series as covariates in a generalized linear model framework. We accomplish
120 this task by building upon the Bayesian nonparametric Skygrid model of Gill et al. (2013).
121 The Skygrid is a particularly well-suited starting point among nonparametric
122 coalescent-based models. In most other comparable models, the trajectory change-points
123 must correspond to internal nodes of the genealogy, creating a hurdle for modeling
124 associations with covariates that are measured at fixed times. The Skygrid bypasses such
125 difficulties by allowing users to specify change-points, providing a more natural framework

126 for our extension. Furthermore, the Skygrid’s Gaussian Markov random field (GMRF)
127 smoothing prior is highly generalizable and affords a straightforward extension to include
128 covariates.

129 We demonstrate the utility of incorporating covariates into demographic inference
130 on four examples. First, we find striking similarities between the demographic and spatial
131 expansion of raccoon rabies in North America. Second, we compare and contrast the
132 epidemiological dynamics of dengue in Puerto Rico with patterns of viral diversity. Third,
133 we examine the population history of the HIV-1 CRF02_AG clade in Cameroon and find
134 that the effective population size is more reflective of HIV incidence than prevalence.
135 Finally, we explore the relationship between musk ox population dynamics and climate
136 change during the Late Quaternary period. Our extension to the Skygrid proves to be a
137 useful framework for ascertaining the association between effective population size and
138 external covariates while accounting for demographic uncertainty. Furthermore, we show
139 that incorporating covariates into the demographic inference framework can improve
140 estimates of effective population size trajectories, increasing precision and uncovering
141 patterns in the population history that integrate the covariate data in addition to the
142 sequence data.

143 METHODS

144 We begin with an overview of coalescent theory and follow with a detailed
145 development of the Skygrid inference framework before presenting its extension that
146 incorporates external covariate data. Readers interested in previewing our approach to
147 include covariates may skip to the section *Incorporating Covariates*. However, we
148 encourage readers who are unfamiliar with the Skygrid to proceed in order.

149 *Coalescent Theory*

150 Consider a random sample of n individuals arising from a classic Fisher-Wright
151 population model of constant size N_e . The coalescent (Kingman 1982a,b) is a stochastic
152 process that generates genealogies relating such a sample. The process begins at the
153 sampling time of all n individuals, $t = 0$, and proceeds backward in time as t increases,
154 successively merging lineages until all lineages have merged and we have reached the root
155 of the genealogy, which corresponds to the most recent common ancestor (MRCA) of the
156 sampled individuals. The merging of lineages is called a coalescent event and there are
157 $n - 1$ coalescent events in all. Let t_k denote the time of the $(n - k)^{\text{th}}$ coalescent event for
158 $k = 1, \dots, n - 1$ and $t_n = 0$ denote the sampling time. Then for $k = 2, \dots, n$, the waiting
159 time $w_k = t_{k-1} - t_k$ is exponentially distributed with rate $\frac{k(k-1)}{2N_e}$.

160 Researchers have extended coalescent theory to model the effects of recombination
161 (Hudson 1983), population structure (Notohara 1990), and selection (Krone and Neuhauser
162 1997). We do not, however, incorporate any of these extensions here. The relevant
163 extensions for our development generalize the coalescent to accommodate a variable
164 population size (Griffiths and Tavaré 1994) and heterochronous data (Rodrigo and
165 Felsenstein 1999). The latter occurs when the n individuals are sampled at two or more
166 different times.

167 Let $N_e(t)$ denote the effective population size as a function of time, where time
168 increases into the past. Thus, $N_e(0)$ is the effective population size at the most recent
169 sampling time, and $N_e(t')$ is the effective population size t' time units before the most
170 recent sampling time. We also refer to $N_e(t)$ as the “demographic function” or
171 “demographic model.” Griffiths and Tavaré (1994) show that the waiting time w_k between
172 coalescent events is given by the conditional density

$$173 \quad P(w_k|t_k) = \frac{k(k-1)}{2N_e(w_k + t_k)} \exp \left[- \int_{t_k}^{w_k+t_k} \frac{k(k-1)}{2N_e(t)} dt \right]. \quad (1)$$

174 Taking the product of such densities yields the joint density of intercoalescent waiting
175 times, and this fact can be exploited to obtain the probability of observing a particular
176 genealogy given a demographic function.

177 *Skygrid Demographic Model*

178 The Skygrid posits that $N_e(t)$ is a piecewise constant function that can change
179 values only at pre-specified points in time known as “grid points.” Let x_1, \dots, x_M denote
180 the temporal grid points, where $x_1 \leq x_2 \leq \dots \leq x_{M-1} \leq x_M$. The M grid points divide the
181 demographic history timeline into $M + 1$ intervals so that the demographic function is fully
182 specified by a vector $\boldsymbol{\theta} = (\theta_1, \dots, \theta_{M+1})$ of values that it assumes on those intervals. Here,
183 $N_e(t) = \theta_k$ for $x_{k-1} \leq t < x_k$, $k = 1, \dots, M$, where it is understood that $x_0 = 0$. Also,
184 $N_e(t) = \theta_{M+1}$ for $t \geq x_M$. Note that x_M is the time furthest back into the past at which
185 the effective population size can change. The values of the grid points as well as the
186 number M of total grid points are specified beforehand by the user. A typical way to select
187 the grid points is to decide on a resolution M , let x_M assume the value furthest back in
188 time for which the data are expected to be informative, and space the remaining grid
189 points evenly between $x_0 = 0$ and x_M . Alternatively, as discussed in the next section, grid
190 points can be selected to align with covariate sampling times in order to facilitate the
191 modeling of associations between the effective population size and external covariates.

192 Suppose we have m known genealogies g_1, \dots, g_m representing the ancestries of
193 samples from m separate genetic loci with the same effective population size $N_e(t)$. We
194 assume *a priori* that the genealogies are independent given $N_e(t)$. This assumption implies
195 that the genealogies are unlinked which commonly occurs when researchers select loci from
196 whole genome sequences or when recombination is very likely, such as between genes in
197 retroviruses. The likelihood of the vector $\mathbf{g} = (g_1, \dots, g_m)$ of genealogies can then be

198 expressed as the product of likelihoods of individual genealogies:

$$199 \quad P(\mathbf{g}|\boldsymbol{\theta}) = \prod_{i=1}^m P(g_i|\boldsymbol{\theta}). \quad (2)$$

200 To construct the likelihood of genealogy g_i , let t_{0_i} be the most recent sampling time
 201 of sequences contributing to genealogy i and t_{MRCA_i} be the time of the MRCA for locus i .
 202 Let x_{α_i} denote the minimal grid point greater than at least one sampling time in the
 203 genealogy, and x_{β_i} the greatest grid point less than at least one coalescent time. Let
 204 $u_{ik} = [x_{k-1}, x_k]$, $k = \alpha_i + 1, \dots, \beta_i$, $u_{i\alpha_i} = [t_{0_i}, x_{\alpha_i}]$, and $u_{i(\beta_i+1)} = [x_{\beta_i}, t_{\text{MRCA}_i}]$. For each u_{ik}
 205 we let t_{kj} , $j = 1, \dots, r_k$, denote the ordered times of the grid points and sampling and
 206 coalescent events in the interval. With each t_{kj} we associate an indicator ϕ_{kj} which takes a
 207 value of 1 in the case of a coalescent event and 0 otherwise. Finally, let v_{kj} denote the
 208 number of lineages present in the genealogy in the interval $[t_{kj}, t_{k(j+1)}]$. Following Griffiths
 209 and Tavaré (1994), the likelihood of observing an interval is

$$210 \quad P(u_{ik}|\theta_k) = \prod_{1 \leq j < r_k: \phi_{kj}=1} \frac{v_{kj}(v_{kj} - 1)}{2\theta_k} \prod_{j=1}^{r_k-1} \exp \left[-\frac{v_{kj}(v_{kj} - 1)(t_{k(j+1)} - t_{kj})}{2\theta_k} \right], \quad (3)$$

211 for $k = \alpha_i, \dots, \beta_i + 1$.

212 The product of interval likelihoods (3) yields the likelihood of coalescent times given
 213 the sampling times associated with genealogy g_i . However, identical coalescent times can
 214 arise from distinct genealogies. Immediately prior to a coalescent time $t_{k(j+1)}$, there are v_{kj}
 215 distinct lineages and therefore $\frac{v_{kj}(v_{kj}-1)}{2}$ different pairs of lineages that can merge and result
 216 in a coalescent event at time $t_{k(j+1)}$. The different possible mergings correspond to different
 217 genealogies. To obtain the likelihood of a particular genealogy we must account for the fact
 218 that a specific pair of lineages must merge at each coalescent time. Let $P_*(u_{ik}|\theta_k)$ denote

219 $P(u_{ik}|\theta_k)$ except with factors of the form $\frac{v_{kj}(v_{kj}-1)}{2\theta_k}$ replaced by $\frac{2(2-1)}{2\theta_k} = \frac{1}{\theta_k}$. Then

$$220 \quad P(g_i|\boldsymbol{\theta}) = \prod_{k=\alpha_i}^{\beta_i+1} P_*(u_{ik}|\theta_k). \quad (4)$$

221 We introduce some notation that will facilitate the derivation of a Gaussian
 222 approximation used to construct a Markov chain Monte Carlo (MCMC) transition kernel.
 223 If c_{ik} denotes the number of coalescent events which occur during interval u_{ik} , we can write

$$224 \quad P(g_i|\boldsymbol{\theta}) = \prod_{k=\alpha_i}^{\beta_i+1} \left(\frac{1}{\theta_k}\right)^{c_{ik}} \exp\left[-\frac{SS_{ik}}{\theta_k}\right], \quad (5)$$

225 where the SS_{ik} are appropriate constants. Rewriting this expression in terms of
 226 $\gamma_k = \log(\theta_k)$, we arrive at

$$227 \quad P(g_i|\boldsymbol{\gamma}) = \prod_{k=\alpha_i}^{\beta_i+1} e^{-\gamma_k c_{ik}} \exp[-SS_{ik}e^{-\gamma_k}] = \prod_{k=\alpha_i}^{\beta_i+1} \exp[-\gamma_k c_{ik} - SS_{ik}e^{-\gamma_k}]. \quad (6)$$

228 Invoking conditional independence of genealogies, the likelihood of the vector \mathbf{g} of
 229 genealogies is

$$230 \quad P(\mathbf{g}|\boldsymbol{\gamma}) = \prod_{i=1}^m P(g_i|\boldsymbol{\gamma}) \quad (7)$$

$$231 \quad = \prod_{i=1}^m \prod_{k=\alpha_i}^{\beta_i+1} \exp[-\gamma_k c_{ik} - SS_{ik}e^{-\gamma_k}] \quad (8)$$

$$232 \quad = \exp\left[\sum_{k=1}^{M+1} [-\gamma_k c_k - SS_k e^{-\gamma_k}]\right] \quad (9)$$

233 where $c_k = \sum_{i=1}^m c_{ik}$ and $SS_k = \sum_{i=1}^m SS_{ik}$; here, $c_{ik} = SS_{ik} = 0$ if $k \notin [\alpha_i, \beta_i + 1]$.

234 The Skygrid incorporates the prior assumption that effective population size

235 changes continuously over time by placing a GMRF prior on γ :

$$236 \quad P(\gamma|\tau) \propto \tau^{M/2} \exp \left[-\frac{\tau}{2} \sum_{i=1}^M (\gamma_{i+1} - \gamma_i)^2 \right]. \quad (10)$$

237 This prior does not inform the overall level of the effective population size, just the
 238 smoothness of the trajectory. One can think of the prior as a first-order unbiased random
 239 walk with normal increments. The precision parameter τ determines how much differences
 240 between adjacent log effective population size values are penalized. We assign τ a gamma
 241 prior:

$$242 \quad P(\tau) \propto \tau^{a-1} e^{-b\tau}. \quad (11)$$

243 In the absence of prior knowledge about the smoothness of the effective population size
 244 trajectory, we choose $a = b = 0.001$ so that it is relatively uninformative. Conditioning on
 245 the vector of genealogies, we obtain the posterior distribution

$$246 \quad P(\gamma, \tau|\mathbf{g}) \propto P(\mathbf{g}|\gamma)P(\gamma|\tau)P(\tau). \quad (12)$$

247 *Incorporating Covariates*

248 We can incorporate covariates into our inference framework by adopting a
 249 generalized linear model (GLM) approach. Let Z_1, \dots, Z_P be a set of P predictors. Each
 250 covariate Z_j is observed or measured at $M + 1$ time points, s_1, \dots, s_M, s_{M+1} . Here, s_i
 251 denotes the units of time before the most recent sequence sampling time $s_0 = 0$, and
 252 $s_0 < s_1 < \dots < s_M < s_{M+1}$. Alternatively, the covariate may correspond to time intervals
 253 $[s_0, s_1], \dots, [s_{M-1}, s_M], [s_M, s_{M+1}]$ rather than time points (for example, the yearly
 254 incidence or prevalence of viral infections). In any case, Z_{ij} denotes covariate Z_j at time
 255 point or interval i . Skygrid grid points are chosen to match up with measurement times (or

256 measurement interval endpoints): $x_1 = s_1, \dots, x_M = s_M$. Then $N_e(t) = \theta_k$ for
 257 $x_{k-1} \leq t \leq x_k$, $k = 1, \dots, M$, and $N_e(t) = \theta_{M+1}$ for $t \geq x_M$. In our GLM framework, we
 258 model the effective population size on a given interval as a log-linear function of covariates

$$259 \quad \gamma_k = \log \theta_k = \beta_1 Z_{k1} + \dots + \beta_P Z_{kP} + w_k. \quad (13)$$

260 Here, we can impose temporal dependence by modeling $w = (w_1, \dots, w_{M+1})$ as a zero-mean
 261 Gaussian process. Adopting this viewpoint, we propose the following GMRF smoothing
 262 prior on γ :

$$263 \quad P(\gamma | \mathbf{Z}, \boldsymbol{\beta}, \tau) \propto \tau^{M/2} \exp \left[-\frac{\tau}{2} (\gamma - \mathbf{Z}\boldsymbol{\beta})' \mathbf{Q} (\gamma - \mathbf{Z}\boldsymbol{\beta}) \right]. \quad (14)$$

264 In this prior, \mathbf{Z} is an $(M+1) \times P$ matrix of covariates and $\boldsymbol{\beta}$ is a $P \times 1$ vector of
 265 coefficients representing the effect sizes for the predictors, quantifying their contribution to
 266 γ . Precision \mathbf{Q} is an $(M+1) \times (M+1)$ tri-diagonal matrix with off-diagonal elements
 267 equal to -1 , $Q_{11} = Q_{M+1, M+1} = 1$, and $Q_{ii} = 2$ for $i = 2, \dots, M$. Let γ_{-i} denote the vector
 268 obtained by excluding only the i^{th} component from vector γ . Therefore, conditional on
 269 γ_{-i} , γ_i depends only on its immediate neighbors. Let \mathbf{Z}_i denote the i^{th} row of covariate
 270 matrix \mathbf{Z} . The individual components of γ have full conditionals

$$271 \quad \gamma_1 | \gamma_{-1} \sim N \left(\mathbf{Z}'_1 \boldsymbol{\beta} - \mathbf{Z}'_2 \boldsymbol{\beta} + \gamma_2, \frac{1}{\tau} \right), \quad (15)$$

$$272 \quad \gamma_i | \gamma_{-i} \sim N \left(\mathbf{Z}'_i \boldsymbol{\beta} + \frac{\gamma_{i-1} + \gamma_{i+1} - \mathbf{Z}'_{i-1} \boldsymbol{\beta} - \mathbf{Z}'_{i+1} \boldsymbol{\beta}}{2}, \frac{1}{2\tau} \right) \quad (16)$$

273 for $i = 2, \dots, M$,

$$274 \quad \gamma_{M+1} | \gamma_{-(M+1)} \sim N \left(\mathbf{Z}'_{M+1} \boldsymbol{\beta} - \mathbf{Z}'_M \boldsymbol{\beta} + \gamma_M, \frac{1}{\tau} \right). \quad (17)$$

275 As in the original Skygrid GMRF prior, the precision parameter τ governs the smoothness

276 of the trajectory and is assigned a gamma prior

$$277 \quad P(\tau) \propto \tau^{a-1} e^{-b\tau}. \quad (18)$$

278 To complete the model specification, we place a relatively uninformative multivariate
279 normal prior $P(\boldsymbol{\beta})$ on the coefficients $\boldsymbol{\beta}$. This yields the posterior

$$280 \quad P(\boldsymbol{\gamma}, \boldsymbol{\beta}, \tau | \mathbf{g}, \mathbf{Z}) \propto P(\mathbf{g} | \boldsymbol{\gamma}) P(\boldsymbol{\gamma} | \mathbf{Z}, \boldsymbol{\beta}, \tau) P(\boldsymbol{\beta}) P(\tau). \quad (19)$$

281 *Missing Covariate Data*

282 It is important to have a mechanism for dealing with unobserved covariate values.
283 This is particularly crucial because the population history timeline, which ranges from the
284 most recent sampling time to the time of the MRCA, necessitates observations from a wide
285 and *a priori* unknown time span. Let \mathbf{Z}^{obs} denote the observed covariate values and \mathbf{Z}^{mis}
286 the missing covariate values, so that $\mathbf{Z} = (\mathbf{Z}^{\text{obs}}, \mathbf{Z}^{\text{mis}})$. The missing data can be treated as
287 extra unknown parameters in a Bayesian model, and they can be estimated provided that
288 there is a model that links them to the observed data and other model parameters. We
289 have the factorization

$$290 \quad P(\boldsymbol{\gamma}, \mathbf{Z}^{\text{mis}} | \mathbf{Z}^{\text{obs}}, \boldsymbol{\beta}, \tau) = P(\boldsymbol{\gamma} | \mathbf{Z}^{\text{obs}}, \mathbf{Z}^{\text{mis}}, \boldsymbol{\beta}, \tau) P(\mathbf{Z}^{\text{mis}} | \mathbf{Z}^{\text{obs}}, \boldsymbol{\beta}, \tau), \quad (20)$$

291 and the marginal density $P(\boldsymbol{\gamma} | \mathbf{Z}^{\text{obs}}, \boldsymbol{\beta}, \tau)$ can be recovered by integrating out the missing
292 data. As a starting point, we assume a “missing completely at random” structure, meaning
293 that the probability that a covariate value is missing is independent of observed covariate
294 values and other model parameters. For the priors on missing covariate values in (20), we
295 can adopt uniform distributions over plausible ranges.

296 Alternatively, we can formulate a prior on the missing covariate data that makes use
 297 of the observed covariate values. Here, we focus on a common scenario where covariate j is
 298 observed at times x_1, \dots, x_K and unobserved at times x_{K+1}, \dots, x_{M+1} . Thus, we can write
 299 $\mathbf{Z}_j^{\text{obs}} = (Z_{1j}, \dots, Z_{Kj})'$ and $\mathbf{Z}_j^{\text{mis}} = (Z_{(K+1)j}, \dots, Z_{(M+1)j})'$. We model the joint distribution
 300 of the observed and missing covariate values as multivariate normal,

$$301 \quad \begin{pmatrix} \mathbf{Z}_j^{\text{obs}} \\ \mathbf{Z}_j^{\text{mis}} \end{pmatrix} \sim N \left(\begin{pmatrix} \boldsymbol{\mu}_1 \\ \boldsymbol{\mu}_2 \end{pmatrix}, \begin{pmatrix} \mathbf{P}_{11} & \mathbf{P}_{12} \\ \mathbf{P}_{21} & \mathbf{P}_{22} \end{pmatrix}^{-1} \right), \quad (21)$$

302 where

$$303 \quad \mathbf{P} = \begin{pmatrix} \mathbf{P}_{11} & \mathbf{P}_{12} \\ \mathbf{P}_{21} & \mathbf{P}_{22} \end{pmatrix} \quad (22)$$

304 is the precision matrix. To impose a correlation structure that enforces dependence
 305 between covariate values corresponding to adjacent times, we adopt a first-order random
 306 walk with full conditionals

$$307 \quad Z_{1j} | Z_{-1j} \sim N \left(Z_{2j}, \frac{1}{\kappa} \right), \quad (23)$$

$$308 \quad Z_{ij} | Z_{-ij} \sim N \left(\frac{Z_{(i-1)j} + Z_{(i+1)j}}{2}, \frac{1}{2\kappa} \right) \quad (24)$$

309 for $i = 2, \dots, M$,

$$310 \quad Z_{(M+1)j} | Z_{-(M+1)j} \sim N \left(Z_{Mj}, \frac{1}{\kappa} \right). \quad (25)$$

311 Let \mathbf{Z}^K denote a vector of dimension $M - K$ with every entry equal to Z_{Kj} . Then the
 312 distribution of missing covariate values conditional on observed covariate values is

$$313 \quad P(\mathbf{Z}_j^{\text{mis}} | \mathbf{Z}_j^{\text{obs}}) \propto \kappa^{(M-K)/2} \exp \left(-\frac{\kappa}{2} (\mathbf{Z}_j^{\text{mis}} - \mathbf{Z}^K)' \mathbf{P}_{22} (\mathbf{Z}_j^{\text{mis}} - \mathbf{Z}^K) \right), \quad (26)$$

314 where

$$315 \quad \mathbf{P}_{22} = \begin{pmatrix} -1 & 2 & -1 & & \\ & \ddots & \ddots & & \\ & & -1 & 2 & -1 \\ & & & & -1 & 1 \end{pmatrix}. \quad (27)$$

316 This technique of positing a random walk covariate distribution and recovering appropriate
317 conditional distributions can also be employed for other missing data patterns.

318 *Markov Chain Monte Carlo Sampling Scheme*

319 We use MCMC sampling to approximate the posterior

$$320 \quad P(\boldsymbol{\gamma}, \boldsymbol{\beta}, \tau | \mathbf{g}, \mathbf{Z}) \propto P(\mathbf{g} | \boldsymbol{\gamma}) P(\boldsymbol{\gamma} | \mathbf{Z}, \boldsymbol{\beta}, \tau) P(\boldsymbol{\beta}) P(\tau). \quad (28)$$

321 To sample $\boldsymbol{\gamma}$ and τ , we propose a fast-mixing, block-updating MCMC sampling scheme for
322 GMRFs (Knorr-Held and Rue 2002). Suppose we have current parameter values
323 $(\boldsymbol{\gamma}^{(n)}, \tau^{(n)})$. First, consider the full conditional density

$$\begin{aligned} 324 \quad P(\boldsymbol{\gamma} | \mathbf{g}, \mathbf{Z}, \boldsymbol{\beta}, \tau) &\propto P(\mathbf{g} | \boldsymbol{\gamma}) P(\boldsymbol{\gamma} | \mathbf{Z}, \boldsymbol{\beta}, \tau) \\ 325 &\propto \exp \left[\sum_{k=1}^{M+1} (-\gamma_k c_k - SS_k e^{-\gamma_k}) \right] \tau^{M/2} \exp \left[-\frac{\tau}{2} (\boldsymbol{\gamma} - \mathbf{Z}\boldsymbol{\beta})' \mathbf{Q} (\boldsymbol{\gamma} - \mathbf{Z}\boldsymbol{\beta}) \right] \\ 326 &= \tau^{M/2} \exp \left[-\frac{\tau}{2} (\boldsymbol{\gamma} - \mathbf{Z}\boldsymbol{\beta})' \mathbf{Q} (\boldsymbol{\gamma} - \mathbf{Z}\boldsymbol{\beta}) - \sum_{k=1}^{M+1} (\gamma_k c_k + SS_k e^{-\gamma_k}) \right] \\ 327 &= \tau^{M/2} \exp \left[-\frac{\tau}{2} \boldsymbol{\gamma}' \mathbf{Q} \boldsymbol{\gamma} + (\mathbf{Z}\boldsymbol{\beta})' \tau \mathbf{Q} \boldsymbol{\gamma} - \sum_{k=1}^{M+1} (\gamma_k c_k + SS_k e^{-\gamma_k}) \right]. \quad (29) \end{aligned}$$

328 Let $h_k(\gamma_k) = (\gamma_k c_k + SS_k e^{-\gamma_k})$. We can approximate each term $h_k(\gamma_k)$ by a second-order

329 Taylor expansion about, say, $\hat{\gamma}_k$:

$$\begin{aligned}
330 \quad h_k(\gamma_k) &\approx h_k(\hat{\gamma}_k) + h'_k(\hat{\gamma}_k)(\gamma_k - \hat{\gamma}_k) + \frac{1}{2}h''_k(\hat{\gamma}_k)(\gamma_k - \hat{\gamma}_k)^2 \\
331 &= SS_k e^{-\hat{\gamma}_k} \left(\frac{1}{2}\hat{\gamma}_k^2 + \hat{\gamma}_k + 1 \right) \\
332 &\quad + [c_k - SS_k e^{-\hat{\gamma}_k} - SS_k e^{-\hat{\gamma}_k} \hat{\gamma}_k] \gamma_k \\
333 &\quad + \left[\frac{1}{2}SS_k e^{-\hat{\gamma}_k} \right] \gamma_k^2. \tag{30}
\end{aligned}$$

334 We center the Taylor expansion about a point $\hat{\boldsymbol{\gamma}} = (\hat{\gamma}_1, \dots, \hat{\gamma}_{M+1})$ obtained iteratively by
335 the Newton-Raphson method:

$$336 \quad \boldsymbol{\gamma}_{(n+1)} = \boldsymbol{\gamma}_{(n)} - [d^2 f(\boldsymbol{\gamma}_{(n)})]^{-1} (df(\boldsymbol{\gamma}_{(n)}))' \tag{31}$$

337 with $\boldsymbol{\gamma}_{(0)} = \boldsymbol{\gamma}^{(n)}$, the current value of $\boldsymbol{\gamma}$. Here,

$$338 \quad f(\boldsymbol{\gamma}) = -\frac{1}{2}\boldsymbol{\gamma}'\boldsymbol{\tau}\mathbf{Q}\boldsymbol{\gamma} + (\mathbf{Z}\boldsymbol{\beta})'\boldsymbol{\tau}\mathbf{Q}\boldsymbol{\gamma} - \sum_{k=1}^{M+1} (\gamma_k c_k + SS_k e^{-\gamma_k}) \tag{32}$$

339 with

$$340 \quad df(\boldsymbol{\gamma}) = -\boldsymbol{\gamma}'\boldsymbol{\tau}\mathbf{Q} + (\mathbf{Z}\boldsymbol{\beta})'\boldsymbol{\tau}\mathbf{Q} - [c_1 - SS_1 e^{-\gamma_1}, \dots, c_{M+1} - SS_{M+1} e^{-\gamma_{M+1}}] \tag{33}$$

341 and

$$342 \quad d^2 f(\boldsymbol{\gamma}) = -\boldsymbol{\tau}\mathbf{Q} - \text{diag}[SS_k e^{-\gamma_k}]. \tag{34}$$

343 Replacing the terms $h_k(\gamma_k)$ with their Taylor expansions yields the following second-order

344 Gaussian approximation to the full conditional density $P(\boldsymbol{\gamma}|\mathbf{g}, \mathbf{Z}, \boldsymbol{\beta}, \tau)$:

345

$$346 \quad P(\boldsymbol{\gamma}|\mathbf{g}, \mathbf{Z}, \boldsymbol{\beta}, \tau) \approx \tau^{M/2} \exp \left[-\frac{1}{2} \boldsymbol{\gamma}' [\tau \mathbf{Q} + \text{Diag}(SS_k e^{-\hat{\gamma}_k})] \boldsymbol{\gamma} + (\tau \mathbf{Q} \mathbf{Z} \boldsymbol{\beta})' \boldsymbol{\gamma} \right. \\ 347 \quad \left. - \sum_{k=1}^{M+1} (c_k - SS_k e^{-\hat{\gamma}_k} - SS_k e^{-\hat{\gamma}_k} \hat{\gamma}_k) \gamma_k \right], \quad (35) \\ 348$$

349 where $\text{Diag}(\cdot)$ is a diagonal matrix.

350 Starting from current parameter values $(\boldsymbol{\gamma}^{(n)}, \tau^{(n)})$, we first generate a candidate
 351 value for the precision, $\tau^* = \tau^{(n)} f$, where f is drawn from a symmetric proposal
 352 distribution with density $P(f) \propto f + \frac{1}{f}$ defined on $[1/F, F]$. The tuning constant F controls
 353 the distance between the proposed and current values of the precision. Next, conditional on
 354 τ^* , we propose a new state $\boldsymbol{\gamma}^*$ using the Gaussian approximation (35) to the full conditional
 355 density $P(\boldsymbol{\gamma}|\mathbf{g}, \mathbf{Z}, \boldsymbol{\beta}, \tau^*)$. In the final step, the candidate state $(\tau^*, \boldsymbol{\gamma}^*)$ is accepted or
 356 rejected according to the Metropolis-Hastings ratio (Metropolis et al. 1953; Hastings 1970).

357

Genealogical Uncertainty

358 In our development thus far, we have assumed the genealogies g_1, \dots, g_m are known
 359 and fixed. However, in reality we observe sequence data rather than genealogies. It is
 360 possible to estimate genealogies beforehand from sequence data and then infer the effective
 361 population size from fixed genealogies. However, this ignores the uncertainty associated
 362 with phylogenetic reconstruction. Alternatively, we can jointly infer genealogies and
 363 population dynamics from sequence data by combining the estimation procedures into a
 364 single Bayesian framework.

365 We can think of the aligned sequence data $\mathbf{Y} = (Y_1, \dots, Y_m)$ for the m loci as
 366 arising from continuous-time Markov chain (CTMC) models for molecular character
 367 substitution that act along the hidden genealogies. Each CTMC depends on a vector of

368 mutational parameters Λ_i , that include, for example, an overall rate multiplier, relative
369 exchange rates among characters and across-site variation specifications. We let
370 $\mathbf{\Lambda} = (\Lambda_1, \dots, \Lambda_m)$. We then jointly estimate the genealogies, mutational parameters,
371 covariate effect size coefficients, precision, and vector of effective population sizes through
372 their posterior distribution

$$373 \quad P(\mathbf{g}, \mathbf{\Lambda}, \boldsymbol{\beta}, \tau, \boldsymbol{\gamma} | \mathbf{Y}, \mathbf{Z}) \propto \left[\prod_{i=1}^m P(Y_i | g_i, \Lambda_i) \right] P(\mathbf{\Lambda}) P(\mathbf{g} | \boldsymbol{\gamma}) P(\boldsymbol{\gamma} | \mathbf{Z}, \boldsymbol{\beta}, \tau) P(\boldsymbol{\beta}) P(\tau). \quad (36)$$

374 Here, the coalescent acts as a prior for the genealogies, and we assume that $\mathbf{\Lambda}$ and \mathbf{g} are *a*
375 *priori* independent of each other. Hierarchical models are however available to share
376 information about $\mathbf{\Lambda}$ among loci without strictly enforcing that they follow the same
377 evolutionary process (Suchard et al. 2003; Edo-Matas et al. 2011). We implement our
378 models in the open-source software program BEAST v1 (Drummond et al. 2012). The
379 posterior distribution is approximated through MCMC methods. We combine our
380 block-updating scheme for $\boldsymbol{\gamma}$ and τ with standard transition kernels available in BEAST to
381 update the other parameters. The extended Skygrid model will be included in the next
382 official release of BEAST v1. In the meantime, it can be accessed by users through the
383 BEAST v1 development branch source code, which is available at
384 <https://github.com/beast-dev/beast-mcmc/>. Example BEAST XML input files are
385 available as part of the Supplementary Material online
386 (<http://datadryad.org/resource/doi:10.5061/dryad.mj0hn>).

387 EMPIRICAL EXAMPLES

388 *Expansion in Epizootic Rabies Virus*

389 Rabies is a zoonotic disease caused by the rabies virus, and is responsible for over
390 50,000 human deaths annually. In over 99% of human cases, the rabies virus is transmitted
391 by dogs. However, there are a number of other important rabies reservoirs, such as bats
392 and several terrestrial carnivore species, including raccoons (WHO 2015b). Epizootic rabies
393 among raccoons was first identified in the U.S. in Florida in the 1940s, and the affected
394 area of the subsequent expansion was limited to the southeastern U.S. (Kappus et al.
395 1970). A second focus of rabies among raccoons emerged in West Virginia in the late 1970s
396 due to the translocation of raccoons incubating rabies from the southeastern U.S. The
397 virus spread rapidly along the mid-Atlantic coast and northeastern U.S. over the following
398 decades, and is one of the largest documented outbreaks in the history of wildlife rabies
399 (Childs et al. 2000).

400 Biek et al. (2007) examine the population dynamics of the rabies epizootic among
401 raccoons in the northeastern U.S. starting in the late 1970s. In a spatiogenetic analysis,
402 Biek et al. (2007) compare a coalescent-based Bayesian Skyline estimate (Drummond et al.
403 2005) of the demographic history to the spatial expansion of the epidemic. In a *post hoc*
404 approach, the authors find very similar temporal dynamics between the effective
405 population size and the 15-month moving average of the area (in square kilometers) of
406 counties newly affected by the rabies outbreak each month. The effective population size
407 exhibits stages of moderate and rapid growth, as well as plateau periods with little or no
408 growth. Population expansion coincides with time periods during which the virus invades
409 new areas at a generally increasing rate. On the other hand, the effective population size
410 shows little, if any, growth during periods when the virus invades new areas at a declining
411 rate. Notably, Biek et al. (2007) demonstrate through their analysis that the largest
412 contribution to the population expansion comes from the wave front, highlighting the
413 degree to which the overall viral dynamics depend on processes at the wave front. We
414 observe the same trends in a Skygrid demographic reconstruction based on the Biek et al.

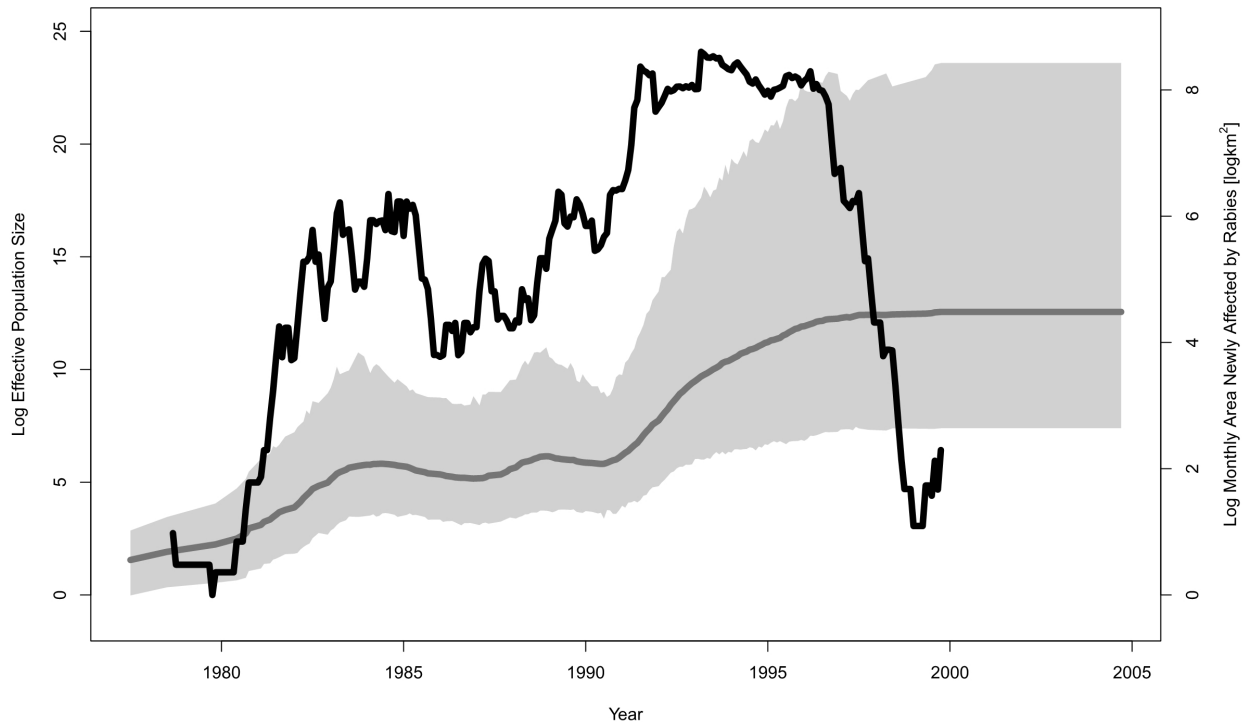


Figure 1: Skygrid demographic reconstruction of raccoon rabies epidemic in the northeastern United States. The gray line is the posterior mean log effective population size trajectory estimated only from sequence data without incorporating covariate data. The shaded gray region is the 95% Bayesian credibility interval region for the log effective population size. The black line represents the covariate, the 15-month moving average of the log-transformed area of all counties newly affected by the raccoon rabies virus each month.

415 (2007) sequence data (Figure 1).

416 We build upon the analysis of Biek et al. (2007) by incorporating the
 417 spatiotemporal spread of rabies into the demographic inference model through the Skygrid.
 418 The sequence data consist of 47 sequences sampled from rabid raccoons between 1982 and
 419 2004. They encompass the complete rabies nucleoprotein (N) genes as well as large
 420 portions of the glycoprotein (G) genes. As a covariate, we initially adopt the 15-month
 421 moving average of the log-transformed area of all counties newly affected by the raccoon
 422 rabies virus each month from 1977-1999 (Biek et al. 2007). We infer a posterior mean

423 covariate effect size of 0.24 with a 95% Bayesian credibility interval (BCI) of (-0.77, 1.27),
424 implying that there is not a significant association between the log effective population size
425 and the covariate. This is not surprising, considering the patterns of growth and decline in
426 the covariate compared with the essentially monotonic trend in the log effective population
427 size (see Figure 1).

428 Graphically comparing the rate at which the virus invades new areas with
429 population dynamics clearly illustrates the relationship between the demographic and
430 spatial expansion of the raccoon rabies outbreak. In modeling the association between the
431 population dynamics and a covariate, however, we relate the covariate to the total effective
432 population size (as opposed to the change in the effective population size). In this case, the
433 cumulative affected area is a more suitable covariate than the newly affected area. We
434 conduct an additional Skygrid analysis and use the log-transform of the cumulative area
435 (in square kilometers) of counties affected by raccoon rabies at various time points between
436 1977 and 1999 as a covariate. The area of a county is added to the cumulative total for the
437 month during which rabies is first reported in that county. There are 175 months for which
438 the cumulative affected area changes, and we specify the grid points to coincide with these
439 change points.

440 The Skygrid analysis with the log cumulative affected area covariate yields a
441 posterior mean estimate of 1.30 for the coefficient β , with a 95% BCI of (0.18, 2.86),
442 implying a significant, positive association between the effective population size of the
443 raccoon rabies virus and the cumulative area affected by the outbreak (Figure 2). Periods
444 of demographic expansion are marked by relatively rapid rates of increase in the affected
445 area, while plateaus in the effective population size coincide with more modest rates of
446 increase in the affected area. The effective population size trajectory estimated from both
447 sequence and covariate data displays nearly identical patterns to the trajectory estimated
448 only from sequence data, except from 1990-1996, when its rate of increase is more modest.

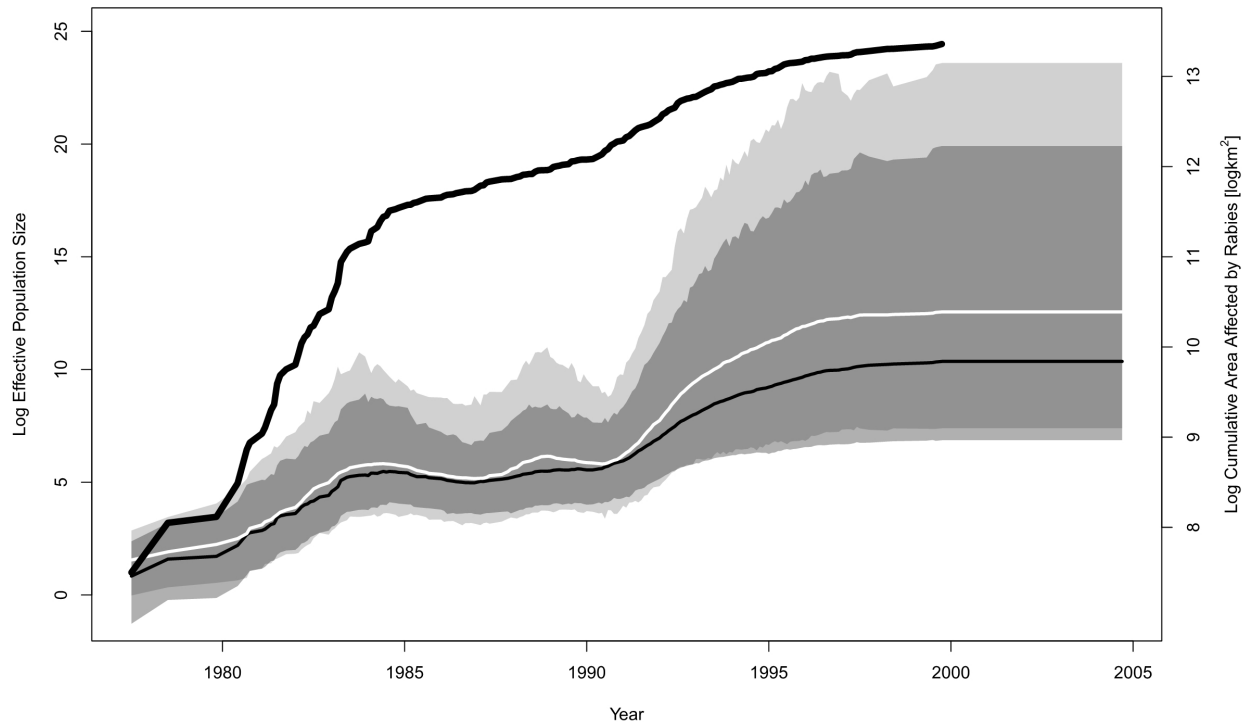


Figure 2: Demographic history of raccoon rabies epidemic in the northeastern United States. The black line that extends outside the shaded regions represents the covariate, the log cumulative area of counties affected by raccoon rabies virus. The black line contained within the shaded regions is the posterior mean log effective population size trajectory from the Skygrid analysis with the covariate, and the surrounding shaded dark gray region is its 95% Bayesian credibility interval (BCI) region. The white line is the posterior mean log effective population size trajectory from the Skygrid analysis without the covariate, and the surrounding shaded light gray region is its 95% BCI region. The two BCI regions overlap considerably, and the dark gray BCI region is almost entirely contained within the light gray BCI region.

449 Notably, the dark gray BCI region inferred from the sequence and covariate data is
450 narrower than and virtually entirely contained within the light gray BCI region inferred
451 only from the sequence data. Thus including the covariate in this analysis not only yields
452 an estimate consistent with what we infer from the sequence data alone, but also a more
453 precise estimate.

454 *Epidemic Dynamics in Dengue Evolution*

455 Dengue is a mosquito-borne viral infection that causes a severe flu-like illness in
456 which potentially lethal syndromes occasionally arise. Dengue is caused by the dengue
457 virus, DENV, an RNA virus which comes in four antigenically distinct but closely related
458 serotypes, DENV-1 through DENV-4. (WHO 2015a). A recent estimate places the
459 worldwide burden of dengue at 390 million infections per year (with 95% confidence
460 interval 284-528 million), of which 96 million (67-136 million) manifest clinically (with any
461 level of disease severity) (Bhatt et al. 2013). Dengue is found in tropical and sub-tropical
462 climates throughout the world, mostly in urban and semi-urban areas (WHO 2015a).

463 Dengue incidence records often show patterns of periodicity with outbreaks every
464 3-5 years (Cummings et al. 2004; Adams et al. 2006; Bennett et al. 2010). Studies have
465 shown that the epidemiological dynamics of dengue transmission in Puerto Rico are
466 reflective of changes in the viral effective population size (Bennett et al. 2010; Carrington
467 et al. 2005). Bennett et al. (2010) explore the dynamics of DENV-4 in Puerto Rico from
468 1981-1998. By *post hoc* comparing dengue isolate counts to effective population size
469 estimates obtained using the Skyride model (Minin et al. 2008), Bennett et al. (2010) show
470 that the pattern of cyclic epidemics is highly correlated with similar fluctuations in genetic
471 diversity. We build upon their analysis by inferring the effective population size of DENV-4
472 in Puerto Rico with DENV-4 isolate counts as a covariate.

473 We analyze a data set of 75 DENV-4 sequences, compiled by Bennett et al. (2003)
474 through sequencing randomly selected DENV-4 isolates from Puerto Rico from the U.S.
475 Centers for Disease Control and Prevention (CDC) sample bank. Each sequence contains
476 gene regions amounting to 40% of the viral genome, including all structural genes (capsid:
477 *C*; membrane: *M*; and envelope: *E*), a subset of nonstructural genes (*NS1*, *NS2A*, and
478 *NS4B*), and the noncoding 3' NTR region. The sampling dates include 1982 ($n = 14$),
479 1986/1987 ($n = 19$), 1992 ($n = 15$), 1994 ($n = 14$), and 1998 ($n = 13$). The covariate data
480 consist of the number of DENV-4 isolates recorded over every 6-month period from
481 1981-1998. DENV-4 isolate counts are transformed via the map $x \mapsto \log(x + 1)$ (this
482 specific logarithmic transformation is chosen to accommodate the transformation of isolate
483 counts of zero).

484 The patterns in the Skygrid demographic reconstructions are generally consistent
485 with the isolate count fluctuations, and suggest a periodicity of 3-5 years (Figure 3). This
486 concordance is supported by a positive, statistically significant estimate of the coefficient β
487 relating the effective population size to isolate counts: a posterior mean of 0.90 with 95%
488 BCI (0.36, 1.69).

489 The effective population size trajectory inferred from both sequence and covariate
490 data is similar to the trajectory estimated only from sequence data, but there are some
491 notable differences. The black-colored estimate that incorporates covariate data closely
492 reflects the DENV-4 isolate count patterns, but the white-colored trajectory inferred
493 entirely from sequence data diverges from the isolate count trends during certain periods.
494 First, the white trajectory shows a dramatic increase in effective population size in 1981,
495 consistent with a rise in DENV-4 isolates. However, the white trajectory decreases during
496 1982 while the DENV-4 isolate counts remain at a high level. Second, the period from late
497 1986 to late 1988 begins and ends with relative peaks in DENV-4 isolates, with a trough in
498 between. By contrast, the white curve reaches a peak during the isolate trough and is on

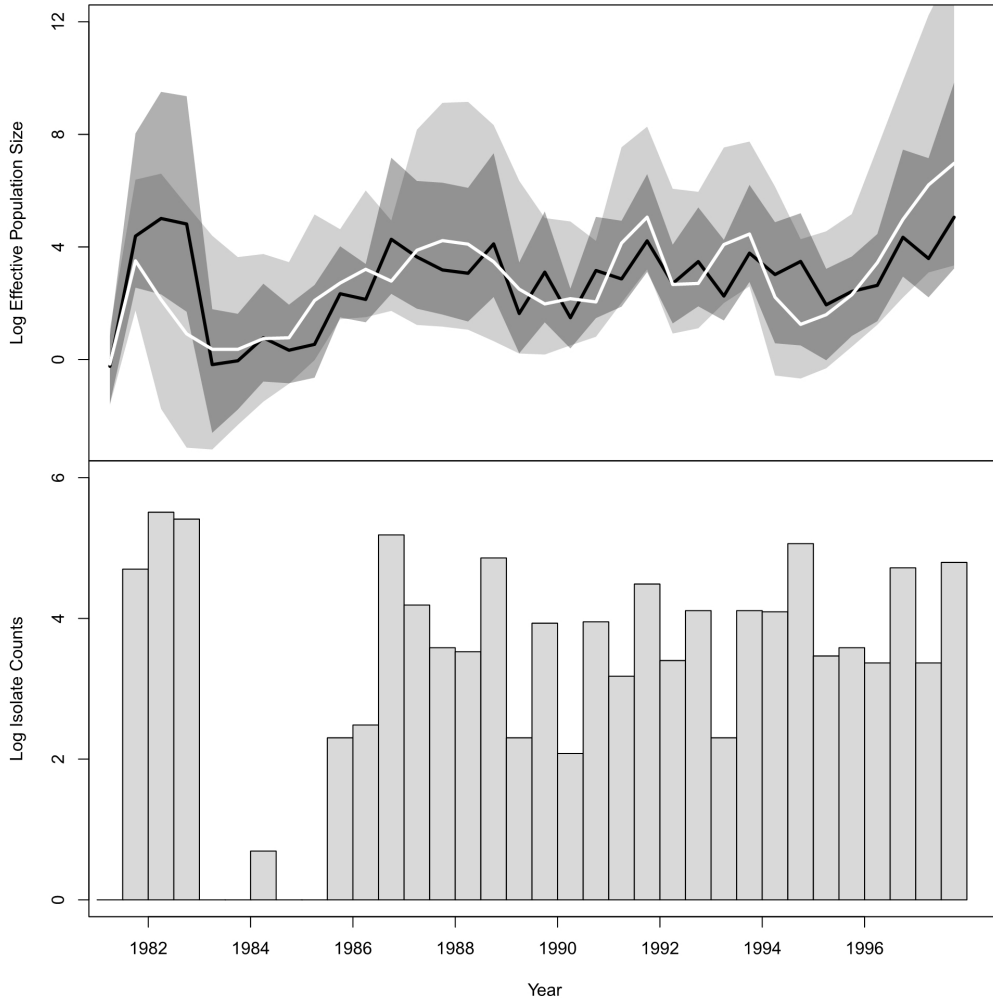


Figure 3: Population and epidemiological dynamics of DENV-4 virus in Puerto Rico. The top plot depicts Skygrid effective population size estimates. The black line is the posterior mean log effective population size trajectory from the Skygrid analysis with the covariate, and the surrounding shaded dark gray region is its 95% Bayesian credibility interval (BCI) region. The white line is the posterior mean log effective population size trajectory from the Skygrid analysis without the covariate, and the surrounding shaded light gray region is its 95% BCI region. The two BCI regions overlap considerably, and the dark gray BCI region is almost entirely contained within the light gray BCI region. The bars in the bottom plot represent DENV-4 isolate count covariate data.

499 the decline during the late 1988 peak. Third, the white trajectory shows a trough in the
500 effective population size during 1994 that occurs about a year before a similar trough in
501 DENV-4 isolates. These discrepancies may be due to biased sampling in isolate counts and
502 reflect limitations of epidemiological surveillance. Isolate counts are a rough measure of
503 incidence, and their error rates are subject to accurate diagnostic rates by medical
504 personnel, reporting rates, and the rate at which suspected cases are submitted for
505 isolation (Bennett et al. 2010). On the other hand, the epidemiological trends are not
506 necessarily incompatible with the effective population size trajectory estimated entirely
507 from sequence data when the latter's uncertainty is taken into account. The black-colored
508 trajectory inferred from both sequence and isolate count data does not deviate from the
509 isolate count data in the ways that the white trajectory does. However, the black
510 trajectory lies entirely inside the light gray 95% BCI region. Furthermore, apart from a 1.5
511 year period in 1981-82, the dark gray 95% BCI region is virtually entirely contained within,
512 and is narrower than, the light gray 95% BCI region. Therefore, the Skygrid estimate that
513 incorporates the DENV-4 isolate count covariate yields a demographic pattern that reflects
514 epidemiological dynamics, and is more precise than, but not incompatible with, the
515 effective population size estimate inferred only from sequence data.

516 *Demographic History of the HIV-1 CRF02_AG Clade in Cameroon*

517 Circulating recombinant forms (CRFs) are genomes that result from recombination
518 of two or more different HIV-1 subtypes and that have been found in at least three
519 epidemiologically unrelated individuals. Although CRF02_AG is globally responsible for
520 only 7.7% of HIV infections (Hemelaar et al. 2011), it accounts for 60-70% of infections in
521 Cameroon (Brennan et al. 2008; Powell et al. 2010).

522 We investigate the population history of the CRF02_AG clade in Cameroon by
523 examining a multilocus alignment of 336 *gag*, *pol*, and *env* CRF02_AG gene sequences

524 sampled between 1996 and 2004 from blood donors from Yaounde and Douala (Brennan
525 et al. 2008). Faria et al. (2012) infer the effective population size from this data set with a
526 parametric piecewise logistic growth-constant demographic model. Their results point to a
527 period of exponential growth up until the mid 1990s, at which point the effective
528 population size plateaus. Gill et al. (2013) follow up with a nonparameteric Skygrid analysis
529 that reveals a monotonic growth in effective population size that peaks around 1997 and is
530 then followed by a decline (rather than a plateau) that persists up until the most recent
531 sampling time. We build upon these analyses by introducing two covariates: the yearly
532 prevalence of HIV in Cameroon among adults ages 18-49, and the yearly HIV incidence rate
533 in Cameroon among adults ages 18-49 (UNAIDS 2015). UNAIDS prevalence and incidence
534 estimates for Cameroon only go back to 1990, so we integrate out the missing covariate
535 values as described in (26) by modeling the covariate values as a first-order random walk.

536 The HIV prevalence increases up until 2000, stays constant for 4 years, and then
537 declines slightly in 2004. This differs markedly from the effective population size temporal
538 pattern (Figure 4), and this discordance is reflected in the GLM coefficient quantifying the
539 prevalence effect size. The coefficient has a posterior mean of 0.85 with 95% BCI (-0.18,
540 2.03), indicating no significant association between the effective population size and
541 prevalence.

542 The coefficient quantifying the effect size for the incidence rate covariate has a
543 posterior mean of 9.20 with 95% BCI (1.43, 16.17), implying a significant association
544 between the population history of the CRF02_AG clade and the HIV incidence rate among
545 adults ages 18-49 in Cameroon. The effective population size and incidence rate display
546 similar dynamics: both increase up until a peak around 1997, then decline (Figure 5). The
547 posterior mean log effective population size and 95% BCI under the Skygrid model without
548 covariates are virtually the same as the Skygrid estimates that incorporate the incidence
549 data. This is in contrast to the previous examples we've seen, where inclusion of covariates

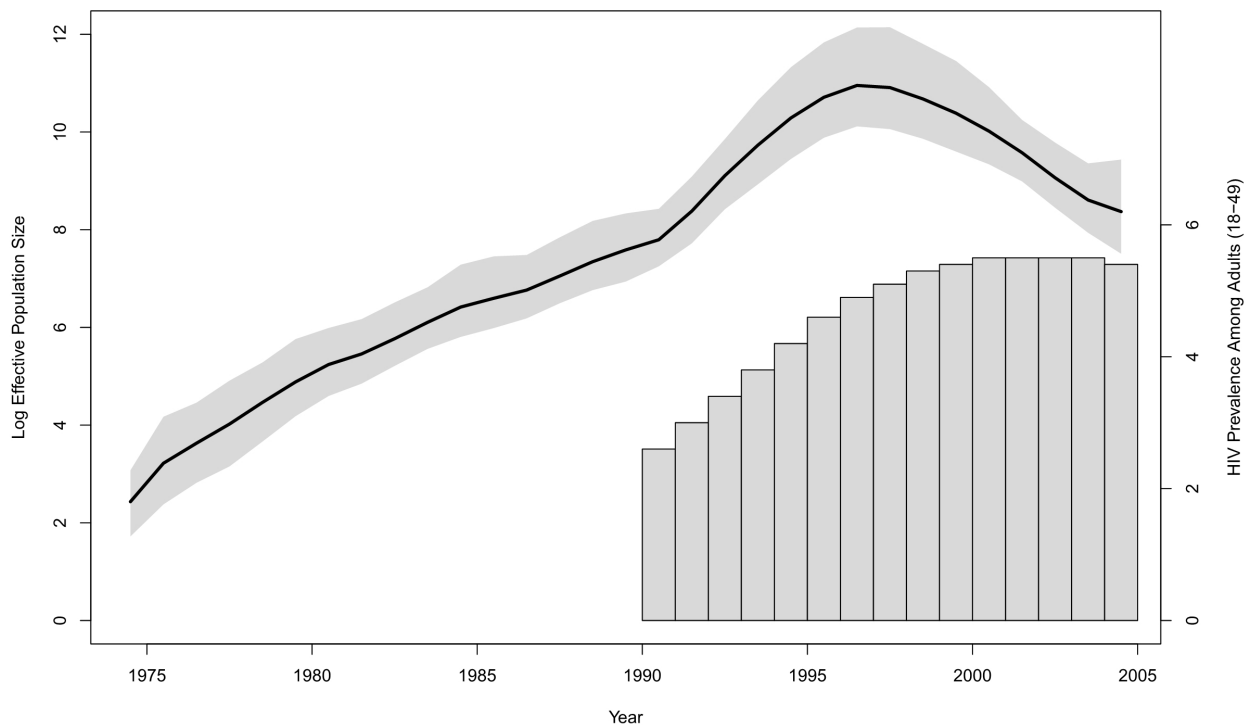


Figure 4: Demographic history of HIV-1 CRF02_AG clade in Cameroon. The black line is the posterior mean log effective population size trajectory, and its 95% Bayesian credibility interval region is shaded in gray. The bars represent HIV prevalence estimates for adults of ages 18-49 in Cameroon.

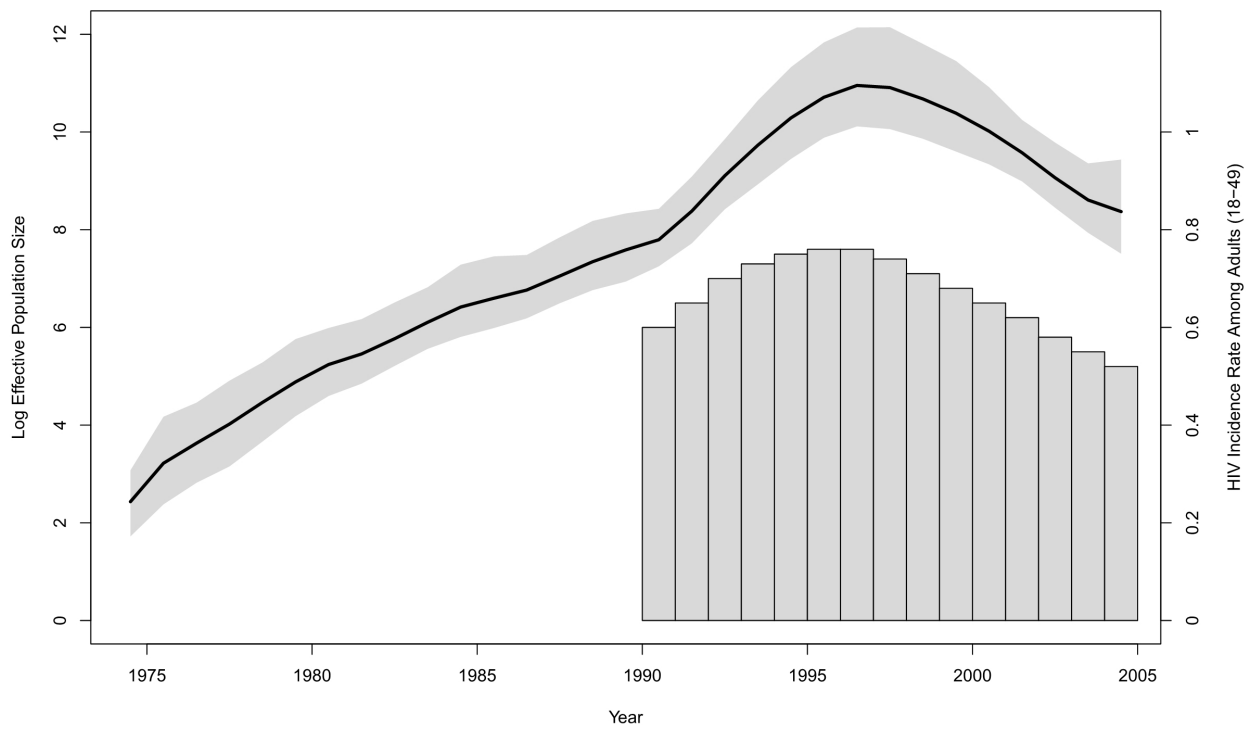


Figure 5: Demographic history of HIV-1 CRF02_AG clade in Cameroon. The black line is the posterior mean log effective population size trajectory, and its 95% Bayesian credibility interval region is shaded in gray. The bars represent HIV incidence rate estimates for adults of ages 18-49 in Cameroon.

550 affects effective population size estimates, and it may reflect the larger amount of sequence
551 data relative to covariate data in this example. It is notable that in this example the
552 effective population size is more reflective of incidence than prevalence. This is in
553 accordance with expectations put forth by recent epidemiological modeling of infectious
554 disease dynamics (Volz et al. 2009; Frost and Volz 2010).

555 *Population Dynamics of Late Quaternary Musk Ox*

556 Population decline and extinction of large-bodied mammals characterizes the Late
557 Quaternary period (Barnosky et al. 2004; Lorenzen et al. 2011). The causes of these
558 megafaunal extinctions remain poorly understood, and much of the debate revolves around
559 the impact of climate change and humans (Stuart et al. 2004; Lorenzen et al. 2011).
560 Demographic reconstructions from ancient DNA enable clarification of the roles of climatic
561 and anthropogenic factors by providing a means to compare demographic patterns over
562 geologically significant time scales with paleoclimatic and fossil records (Shapiro et al.
563 2004; Lorenzen et al. 2011).

564 Campos et al. (2010) employ the Skyride (Minin et al. 2008) and Bayesian Skyline
565 (Drummond et al. 2005) models to reconstruct the population dynamics of musk ox dating
566 back to the late Pleistocene era from ancient DNA sequences. The musk ox population was
567 once widely distributed in the Holarctic ecozone but is now confined to Greenland and the
568 Arctic Archipelago, and Campos et al. (2010) explore potential causes of musk ox
569 population decline. The authors find that the arrival of humans into relevant areas did not
570 correspond to changes in musk ox effective population size. On the other hand, Campos
571 et al. (2010) observe that time intervals during which musk ox populations increase
572 generally correspond to periods of global climatic cooling, and musk ox populations decline
573 during warmer and climatically unstable periods. Thus environmental change, as opposed

574 to human presence, emerges as a more promising candidate as a driving force behind musk
575 ox population dynamics.

576 We apply our extended Skygrid model to assess the relationship between the
577 population history of musk ox and climate change. Oxygen isotope records serve as useful
578 proxies for temperature in ancient climate studies. Here, we use ice core $\delta^{18}\text{O}$ data from
579 the Greenland Ice Core Project (GRIP) (Johnsen et al. 1997; Dansgaard et al. 1993; GRIP
580 Members 1993; Grootes et al. 1993; Dansgaard et al. 1989). $\delta^{18}\text{O}$ is a measure of oxygen
581 isotope composition. In the context of ice core data, lower $\delta^{18}\text{O}$ values correspond to colder
582 polar temperatures. As a covariate, we adopt a mean $\delta^{18}\text{O}$ value, taking the average of $\delta^{18}\text{O}$
583 values corresponding to each 3,000-year interval. The sequence data consist of 682 bp of
584 the mitochondrial control region, obtained from 149 radiocarbon dated specimens (Campos
585 et al. 2010). The ages of the specimens range from the present to 56,900 radiocarbon (^{14}C)
586 years before present (YBP). The sampling locations span the demographic range of ancient
587 musk ox, with samples from the Taimyr Peninsula ($n = 54$), the Urals ($n = 26$), Northeast
588 Siberia ($n = 12$), North America ($n = 14$) and Greenland ($n = 43$).

589 During each time period that coincides with a monotonically increasing effective
590 population size, the $\delta^{18}\text{O}$ covariate undergoes a net decrease (Figure 6), which suggests a
591 general trend of cooling. On the other hand, periods of monotonic demographic decline
592 coincide with either a covariate increase (indicative of a warming climate) or covariate
593 fluctuations without any clear trends (suggesting climatic instability). These patterns are
594 consistent with the observations of Campos et al. (2010). However, the covariate effect size
595 has a posterior mean of -0.09 with a 95% BCI of (-0.50, 0.35), indicating that there is not a
596 significant association between the log effective population size and the $\delta^{18}\text{O}$ covariate.
597 This is not surprising upon further reflection. The net change in the covariate from the
598 beginning to the end of each monotonic phase of the population trajectory lends some
599 support to the hypothesis of a negative relationship between the effective population size

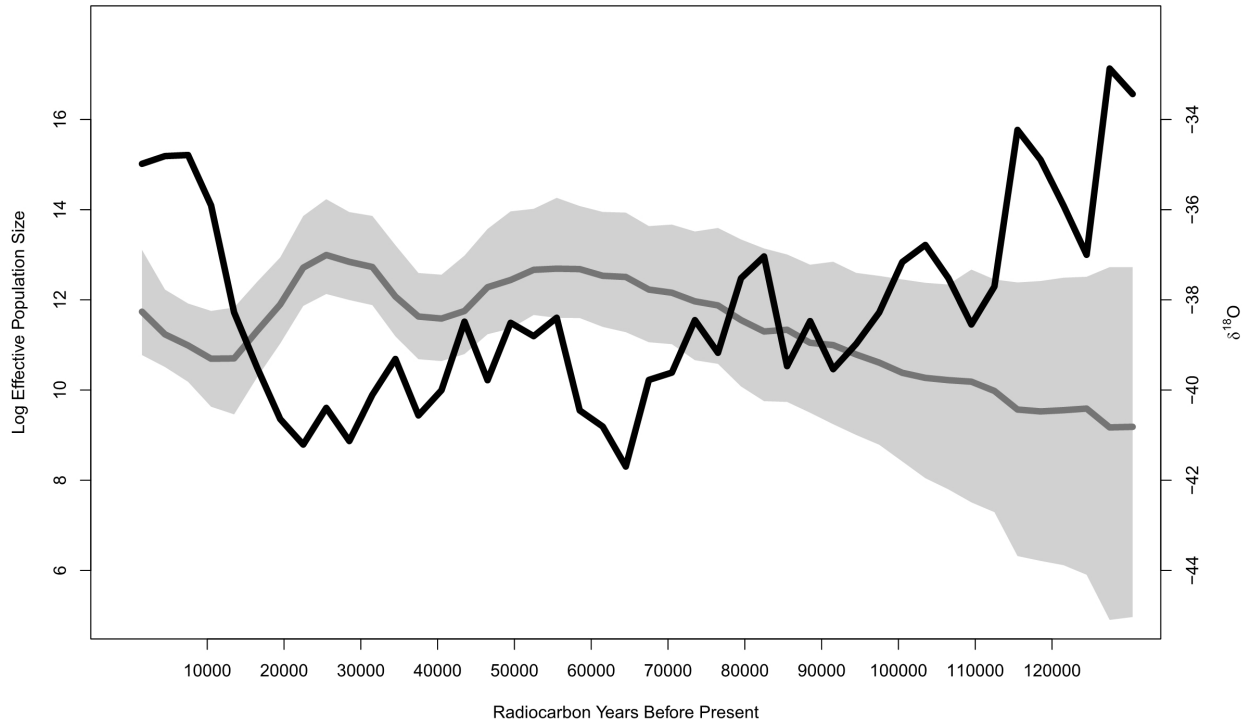


Figure 6: Demographic history of ancient musk ox. The axis is labelled according to radiocarbon years before present. The gray line is the posterior mean log effective population size trajectory, and its 95% Bayesian credibility interval region is shaded in light gray. The black line represents the $\delta^{18}\text{O}$ covariate. We do not infer a significant relationship between the effective population size and the covariate.

600 and the $\delta^{18}\text{O}$ covariate. However, there are numerous fluctuations in the covariate value
 601 during most of the aforementioned phases that render the relationship insignificant.

602 There are more than 5,000 $\delta^{18}\text{O}$ measurements in the GRIP data corresponding to
 603 different time points in the musk ox population history timeline. Our default approach is
 604 to specify Skygrid grid points so that the trajectory has as many piecewise constant
 605 segments as there are covariate measurement times. To avoid having an inappropriately
 606 large number of change points, however, we've used the average of $\delta^{18}\text{O}$ values
 607 corresponding to each 3,000-year interval in the timeline as a covariate. Notably, adopting
 608 averages over intervals of lengths 1,000, 5,000, or 10,000 years as covariates yields the same

634 more basic Metropolis-Hastings transition kernels. The block-updating scheme exploits the
635 structure of the GMRF smoothing prior. Under the more basic approach, we consider a
636 random walk transition kernel for effective population size parameters that proposes new
637 values by adding a random value within a specified window size to the current parameter
638 value. For the precision, we generate candidate values by multiplying the current parameter
639 value by a random scaling factor drawn from a specified window size. The block-updating
640 algorithm consistently outperforms the random walk and rescaling transition kernels.
641 Notably, the MCMC chain generated under the more basic transition kernels fails to
642 generate sufficient ESS after 100 million iterations in the case of the rabies example. All
643 analyses were conducted on a 2.7 GHz Intel Core i5 processor with 8 GB of RAM.

Table 1: Mixing of model parameters in terms of effective sample size (ESS) estimates per minute and fold-improvement in mixing due to a block-updating MCMC algorithm. For effective population size parameters, we report min-max range of ESS per minute. Fold-improvement due to block-updating is relative to more basic transition kernels.

Example	ESS per min.			Fold-improvement	
	Eff. pop. size	Precision	Effect size	Eff. pop. size	Precision
Rabies	12.6 - 53.0	35.7	33.1	165.6 - 252.0 ×	649.7 ×
Dengue	2.2 - 36.2	16.7	2.0	3.5 - 4.2 ×	22.9 ×
HIV	0.3 - 4.4	4.3	1.1	1.2 - 2.4 ×	4.2 ×
Musk ox	5.1 - 66.7	19.1	13.0	1.6 - 3.3 ×	5.3 ×

644 DISCUSSION

645 We present a novel coalescent-based Bayesian framework for estimation of effective
646 population size dynamics from molecular sequence data and external covariates. We
647 achieve this by extending the popular Skygrid model to incorporate covariates. In doing so,
648 we retain the key elements of the Skygrid: a flexible, nonparametric demographic model,

649 smoothing of the trajectory via a GMRF prior, and accommodation of sequence data from
650 multiple genetic loci.

651 Effective population size is of fundamental interest in population genetics, infectious
652 disease epidemiology, and conservation biology. It is crucial to identify explanatory factors,
653 and to achieve a greater understanding of the association between the effective population
654 size and such factors. In the context of viruses, it is important to assess the relationship
655 between effective population size and epidemiological dynamics characterizing the number
656 of infections and the spatiotemporal spread of an outbreak. Our extended Skygrid
657 framework enables formal testing and characterization of such associations.

658 We showcase our methodology in four examples. Our analysis of the raccoon rabies
659 epidemic in the northeastern United States uncovers striking similarities between the viral
660 demographic expansion and the amount of area affected by the outbreak. We reconstruct a
661 cyclic pattern for the effective population size of DENV-4 in Puerto Rico, coinciding with
662 trends in viral isolate count data. Comparing the population history of the HIV-1
663 CRF02_AG clade in Cameroon with HIV incidence and prevalence data reveals a greater
664 alignment with the HIV incidence rate than the prevalence rate. Finally, we consider the
665 role of climate change in ancient musk ox population dynamics by using oxygen isotope
666 data from the GRIP ice core as a proxy for temperature. We do not find a significant
667 association, but our analysis demonstrates the need for a more thorough examination with
668 additional covariates to follow up on previous investigations of the causes of ancient
669 megafaunal population dynamics that consider a number of different factors.

670 Simultaneous inference of the effective population size and its association with
671 covariates enables the uncertainty of the effective population size to be taken into account
672 when assessing the association. Post hoc analyses comparing the mean effective population
673 size trajectory with covariates (employing a standard linear regression approach, for
674 example) are possible. However, such approaches may erroneously rule out significant

675 associations by overemphasizing incompatibilities between the covariates and mean
676 population trajectory. Furthermore, in the case of significant associations, regression
677 coefficient estimates that disregard demographic uncertainty may have inflated precision.

678 Integrating covariates into the demographic inference framework not only enables
679 testing and quantification of associations with the effective population size, it also provides
680 additional information about past population dynamics. In two of our four examples,
681 effective population size trajectories inferred from both sequence and covariate data differ
682 markedly from trajectories inferred only from sequence data. In the rabies and dengue
683 examples, the estimates based on sequence and covariate data are essentially consistent
684 with the estimates from the sequence data (in terms of the former having BCI regions
685 almost entirely contained in the BCI regions of the latter), but more precise and more
686 reflective of covariate trends.

687 It is possible that, in the presence of a statistically significant association between a
688 covariate and the effective population size, the demographic trajectory estimated from
689 sequence and covariate data will exhibit patterns inconsistent with the estimate based
690 strictly on sequence data during a portion of the evolutionary history. This prospect raises
691 concerns that a strong association between a covariate and the effective population size
692 during one time period could cause the demographic history to be poorly estimated during
693 another time period. However, such a scenario will correspond to one of two situations.
694 First, the inconsistency between the two demographic reconstructions occurs for a
695 relatively brief period of time. Second, the inconsistency occurs during a period for which
696 the sequence data provide relatively little information about the population dynamics.
697 Importantly, adding covariates to the model will not distort an originally precise
698 demographic estimate. In our analysis of HIV population dynamics in Cameroon, for
699 example, there is a strong association between the prevalence covariate and demographic
700 history up until the late 1990s that nevertheless does not yield a significant effect size. The

701 sequence data are highly informative about the population dynamics during the early
702 2000s and do not allow for a significant effect size, which would result in a demographic
703 estimate that diverges from the sequence data-based estimate during this period. In
704 general, we recommend performing a sensitivity analysis by estimating the effective
705 population size both with and without covariates and taking note of the duration and
706 nature of inconsistencies between the two estimates. Also, Bayes factors (Jeffreys 1935,
707 1961) can be employed to formally compare the fit of different Skygrid models to observed
708 data (\mathbf{Y}, \mathbf{Z}) . A Bayes factor quantifies the evidence in favor of model M_1 over model M_0 by
709 taking the ratio of marginal likelihoods:

$$710 \quad BF_{10} = \frac{P(\mathbf{Y}, \mathbf{Z}|M_1)}{P(\mathbf{Y}, \mathbf{Z}|M_0)} = \frac{P(M_1|\mathbf{Y}, \mathbf{Z})}{P(M_0|\mathbf{Y}, \mathbf{Z})} \bigg/ \frac{P(M_1)}{P(M_0)}. \quad (37)$$

711 The more general Skygrid model that incorporates covariates includes the more basic
712 Skygrid model as the special case where the effect size $\beta = 0$, affording straightforward
713 computation of Bayes factors.

714 Our extension of the Skygrid represents a first step toward a more complete
715 understanding of past population dynamics, and the utility of the approach as
716 demonstrated in the real data examples is promising. Our examples have only involved one
717 or two covariates, but our implementation can support a large number of predictors.
718 Furthermore, we plan to equip the Skygrid with efficient variable selection procedures to
719 identify optimal subsets of predictors (George and McCulloch 1993; Kuo and Mallick 1998;
720 Chipman et al. 2001). There is considerable potential for further development. For
721 example, there is a prominent correspondence between spatial distribution and genetic
722 diversity in the raccoon rabies example, and in previous studies of megafauna species
723 (Lorenzen et al. 2011). We envision combining the Skygrid with phylogeographic inference
724 models (Bloomquist et al. 2010) to simultaneously infer relevant measures of a population's

725 geographic distribution from sampling location data and use them as predictors to model
726 the effective population size. Such approaches would need to rely on appropriate sampling
727 not only through time, but also through geographic space. Attempts to infer associations
728 between covariates and effective population size dynamics can be hampered by a scarcity of
729 covariate data. Fortunately, there may exist measurements of the same covariates
730 corresponding to different, but similar, genetic sequence data sets. We may, for example,
731 have drug treatment data corresponding to several different HIV patients and wish to
732 assess the relationship between the drug and intrahost HIV evolution. In such a setting,
733 Bayesian hierarchical modeling could enable pooling of information from multiple data sets.
734 Finally, it may be fruitful to develop inference frameworks similar to the Skygrid that are
735 based on generalized coalescent models that incorporate population structure (Notohara
736 1990), recombination (Hudson 1983), and selection (Krone and Neuhauser 1997) to account
737 for different reproductive phenomena and model their associations with external covariates.

738 SUPPLEMENTARY MATERIAL

739 BEAST XML input files for the data analysis are available from the Dryad digital
740 repository: <http://datadryad.org/resource/doi:10.5061/dryad.mj0hn>.

741 FUNDING

742 The research leading to these results has received funding from the European
743 Research Council under the European Community's Seventh Framework Programme
744 (FP7/2007-2013) under Grant Agreement no. 278433-PREDEMICS and ERC Grant
745 agreement no. 260864 and the National Institutes of Health (R01 AI107034, R01
746 HG006139, R01 LM011827 and 5T32AI007370-24) and the National Science Foundation
747 (DMS 1264153). R.B. was supported by NIH grant RO1 AI047498 and the RAPIDD

748 programme of the Science and Technology Directorate of the Department of Homeland
749 Security and NIH Fogarty International Centre.

750 ACKNOWLEDGMENTS

751 We would like to thank the editors, Frank Anderson and Laura Kubatko, as well as
752 David Rasmussen and an anonymous reviewer for constructive comments that helped
753 improve the manuscript.

754 *

755 References

756 Adams, B., E. Holmes, C. Zhang, M. Mammen, S. Nimmannitya, S. Kalayanarooj, and
757 M. Boots. 2006. Cross-protective immunity can account for the alternating epidemic
758 pattern of dengue virus serotypes circulating in Bangkok. *Proceedings of the National
759 Academy of Sciences* 103:14234–14239.

760 Atkinson, Q., R. Gray, and A. Drummond. 2008. mtDNA variation predicts population size
761 in humans and reveals a major Southern Asian chapter in human prehistory. *Molecular
762 Biology and Evolution* 25:468–474.

763 Barnosky, A., P. Koch, R. Feranec, S. Wing, and A. Shabel. 2004. Assessing the causes of
764 Late Pleistocene extinctions on the continents. *Science* 306:70–75.

765 Bazin, E., S. Glemin, and N. Galtier. 2006. Population size does not influence
766 mitochondrial genetic diversity in animals. *Science* 312:570–572.

767 Bennett, S., A. Drummond, D. Kapan, M. Suchard, J. Munoz-Jordan, O. Pybus,
768 E. Holmes, and D. Gubler. 2010. Epidemic dynamics revealed in dengue evolution.
769 *Molecular Biology and Evolution* 27:811–818.

770 Bennett, S., E. Holmes, M. Chirivella, D. Rodriguez, M. Beltran, V. Vorndam, D. Gubler,
771 and W. McMillan. 2003. Selection-driven evolution of emergent dengue virus. *Molecular*
772 *Biology and Evolution* 20:1650–1658.

773 Bhatt, S., P. Gething, O. Brady, J. Messina, A. Farlow, C. Moyes, J. Drake, J. Brownstein,
774 A. Hoen, O. Sankoh, M. Myers, D. George, T. Jaenisch, G. Wint, C. Simmons, T. Scott,
775 J. Farrar, and S. Hay. 2013. The global distribution and burden of dengue. *Nature*
776 496:504–507.

777 Biek, R., J. Henderson, L. Waller, C. Rupprecht, and L. Real. 2007. A high-resolution
778 genetic signature of demographic and spatial expansion in epizootic rabies virus.
779 *Proceedings of the National Academy of Sciences* 104:7993–7998.

780 Bloomquist, E. W., P. Lemey, and M. A. Suchard. 2010. Three roads diverged? routes to
781 phylogeographic inference. *Trends in Ecology & Evolution* 25:626–632.

782 Brennan, C., P. Bodelle, R. Coffey, S. Devare, A. Golden, J. Hackett Jr., B. Harris,
783 V. Holzmayer, K. Luk, G. Schochetman, P. Swanson, J. Yamaguchi, A. Vallari,
784 N. Ndembi, C. Ngansop, F. Makamche, D. Mbanya, L. Gurtler, L. Zekeng, and
785 L. Kaptue. 2008. The prevalence of diverse HIV-1 strains was stable in Cameroonian
786 blood donors from 1996 to 2004. *Journal of Acquired Immune Deficiency Syndrome*
787 49:432–439.

788 Campos, P., E. Willerslev, A. Sher, L. Orlando, E. Axelsson, A. Tikhonov,
789 K. Aaris-Sorenson, A. Greenwood, R. Kahlke, P. Kosintsev, T. Krakhmalnaya,
790 T. Kuznetsova, P. Lemey, R. MacPhee, C. Norris, K. Shepherd, M. Suchard, G. Zazula,
791 B. Shapiro, and M. Gilbert. 2010. Ancient DNA analyses exclude humans as the driving
792 force behind late pleistocene musk ox (*Ovibos moschatus*) population dynamics.
793 *Proceedings of the National Academy of Sciences* 107:5675–5680.

794 Carrington, C., J. Foster, O. Pybus, S. Bennett, and E. Holmes. 2005. Invasion and
795 maintenance of dengue virus type 2 and type 4 in the Americas. *Journal of Virology*
796 79:14680–14687.

797 Childs, J., A. Curns, M. Dey, L. Real, L. Feinstein, and O. Bjornstad. 2000. Predicting the
798 local dynamics of epizootic rabies among raccoons in the United States. *Proceedings of*
799 *the National Academy of Sciences* 97:13666–13671.

800 Chipman, H., E. George, and R. McCulloch. 2001. The practical implementation of
801 Bayesian model selection. *IMS Lecture Notes - Monograph Series* 38:67–134.

802 Crandall, K., D. Posada, and D. Vasco. 1999. Effective population sizes: missing measures
803 and missing concepts. *Animal Conservation* 2:317–319.

804 Cummings, D., R. Irizarry, N. Huang, T. Endy, A. Nisalak, K. Ungchusak, and D. Burke.
805 2004. Travelling waves in the occurrence of dengue haemorrhagic fever in Thailand.
806 *Nature* 427:344–347.

807 Dansgaard, W., S. Johnsen, H. Clausen, D. Dahl-Jensen, N. Gundestrup, C. Hammer,
808 C. Hvidberg, J. Steffensen, A. Sveinbjornsdottir, J. Jouzel, and G. Bond. 1993. Evidence
809 for general instability of past climate from a 250 kyr ice-core record. *Nature* 364:218–220.

810 Dansgaard, W., J. White, and S. Johnsen. 1989. The abrupt termination of the Younger
811 Dryas climate event. *Nature* 339:532–533.

812 Donnelly, P. and S. Tavaré. 1995. Coalescents and genealogical structure under neutrality.
813 *Annual Review of Genetics* 29:401–421.

814 Drummond, A., G. Nicholls, A. Rodrigo, and W. Solomon. 2002. Estimating mutation
815 parameters, population history and genealogy simultaneously from temporally spaced
816 sequence data. *Genetics* 161:1307–1320.

817 Drummond, A., A. Rambaut, B. Shapiro, and O. Pybus. 2005. Bayesian coalescent
818 inference of past population dynamics from molecular sequences. *Molecular Biology and*
819 *Evolution* 22:1185–1192.

820 Drummond, A. J., M. A. Suchard, D. Xie, and A. Rambaut. 2012. Bayesian phylogenetics
821 with beauti and the beast 1.7. *Molecular biology and evolution* 29:1969–1973.

822 Edo-Matas, D., P. Lemey, J. A. Tom, C. Serna-Bolea, A. E. van den Blink, A. B. van't
823 Wout, H. Schuitemaker, and M. A. Suchard. 2011. Impact of CCR5delta32 host genetic
824 background and disease progression on HIV-1 intrahost evolutionary processes: efficient
825 hypothesis testing through hierarchical phylogenetic models. *Molecular Biology and*
826 *Evolution* 28:1605–16.

827 Faria, N., A. Rambaut, M. Suchard, G. Baele, T. Bedford, M. Ward, A. Tatem, J. Sousa,
828 N. Arinaminpathy, J. Pepin, D. Posada, M. Peeters, O. Pybus, and P. Lemey. 2014. The
829 early spread and epidemic ignition of HIV-1 in human populations. *Science* 346:56–61.

830 Faria, N., M. Suchard, A. Abecasis, J. Sousa, N. Ndembi, I. Bonfim, R. Camacho,
831 A. Vandamme, and P. Lemey. 2012. Phylodynamics of the HIV-1 CRF02_AG clade in
832 Cameroon. *Infection, Genetics and Evolution* 12:453–460.

833 Finlay, E., C. Gaillard, S. Vahidi, S. Mirhoseini, H. Jianlin, X. Qi, M. El-Barody, J. Baird,
834 B. Healy, and D. Bradley. 2007. Bayesian inference of population expansions in domestic
835 bovines. *Biology Letters* 3:449–452.

836 Frost, S. and E. Volz. 2010. Viral phylodynamics and the search for an ‘effective number of
837 infections’. *Philosophical Transactions of the Royal Society B* 365:1879–1890.

838 George, E. and R. McCulloch. 1993. Variable selection via Gibbs sampling. *Journal of*
839 *American Statistical Association* 88:881–889.

- 840 Gill, M., P. Lemey, N. Faria, A. Rambaut, B. Shapiro, and M. Suchard. 2013. Improving
841 Bayesian population dynamics inference: a coalescent-based model for multiple loci.
842 *Molecular Biology and Evolution* 30:713–724.
- 843 Griffiths, R. and S. Tavaré. 1994. Sampling theory for neutral alleles in a varying
844 environment. *Philosophical Transactions of the Royal Society of London. Series B,*
845 *Biological Sciences* 344:403–410.
- 846 GRIP Members. 1993. Climate instability during the last interglacial period recorded in
847 the GRIP ice core. *Nature* 364:203–207.
- 848 Grootes, P., M. Stuiver, J. White, S. Johnsen, and J. Jouzel. 1993. Comparison of oxygen
849 isotope records from the GISP2 and GRIP Greenland ice cores. *Nature* 366:552–554.
- 850 Hastings, W. 1970. Monte Carlo sampling methods using Markov chains and their
851 applications. *Biometrika* 57:97–109.
- 852 Heled, J. and A. Drummond. 2008. Bayesian inference of population size history from
853 multiple loci. *BMC Evolutionary Biology* 8:289.
- 854 Hemelaar, J., E. Gouws, P. D. Ghys, S. Osmanov, and WHO-UNAIDS Network for HIV
855 Isolation and Characterisation. 2011. Global trends in molecular epidemiology of HIV-1
856 during 2000-2007. *AIDS* 25:679–89.
- 857 Ho, S. and B. Shapiro. 2011. Skyline-plot methods of estimating demographic history from
858 nucleotide sequences. *Molecular Ecology Resources* 11:423–434.
- 859 Hudson, R. 1983. Properties of a neutral allele model with intragenic recombination.
860 *Theoretical Population Biology* 23:183–201.
- 861 Jeffreys, H. 1935. Some tests of significance, treated by the theory of probability.
862 *Mathematical Proceedings of the Cambridge Philosophical Society* 31:203–222.

863 Jeffreys, H. 1961. *Theory of Probability*. Oxford University Press.

864 Johnsen, S., H. Clausen, W. Dansgaard, N. Gundestrup, C. Hammer, U. Andersen,
865 K. Andersen, C. Hvidberg, D. Dahl-Jensen, J. Steffensen, H. Shoji, A. Sveinbjornsdottir,
866 J. White, J. Jouzel, and D. Fisher. 1997. The d18O record along the Greenland Ice Core
867 Project deep ice core and the problem of possible Eemian climatic instability. *Journal of*
868 *Geophysical Research* 102:26397–26410.

869 Kappus, K., W. Bigler, R. McLean, and H. Trevino. 1970. The raccoon as an emerging
870 rabies host. *Journal of Wildlife Diseases* 6:507–509.

871 Kingman, J. 1982a. The coalescent. *Stochastic Processes and their Applications*
872 13:235–248.

873 Kingman, J. 1982b. On the genealogy of large populations. *Journal of Applied Probability*
874 19:27–43.

875 Knorr-Held, L. and H. Rue. 2002. On block updating in Markov random field models for
876 disease mapping. *Scandinavian Journal of Statistics* 29:597–614.

877 Krone, S. and C. Neuhauser. 1997. Ancestral processes with selection. *Theoretical*
878 *Population Biology* 51:210–237.

879 Kuhner, M., J. Yamato, and J. Felsenstein. 1998. Maximum likelihood estimation of
880 population growth rates based on the coalescent. *Genetics* 149:429–434.

881 Kuo, L. and B. Mallick. 1998. Variable selection for regression models. *Sankhya B*
882 60:65–81.

883 Lemey, P., O. Pybus, B. Wang, N. Saksena, M. Salemi, and A. Vandamme. 2003. Tracing
884 the origin and history of the HIV-2 epidemic. *Proceedings of the National Academy of*
885 *Sciences* 100:6588–6592.

886 Liu, Y. and J. Mittler. 2008. Selection dramatically reduces effective population size in
887 HIV-1 infection. *BMC Evolutionary Biology* 8:133.

888 Lorenzen, E., D. Nogues-Braco, L. Orlando, J. Weinstock, J. Binladen, K. Marske,
889 A. Ugan, M. Borregaard, M. Gilbert, R. Nielsen, S. Ho, T. Goebel, K. Graf, D. Byers,
890 J. Stenderup, M. Rasmussen, P. Campos, J. Leonard, K. Koepfli, D. Froese, G. Zazula,
891 T. Stafford, K. Aaris-Sorensen, P. Batra, A. Haywood, J. Singarayer, P. Valdes,
892 G. Boeskorov, J. Burns, S. Davydov, J. Haile, D. Jenkins, P. Kosintsev, T. Kuznetsova,
893 X. Lai, L. Martin, H. McDonald, D. Mol, M. Meldgaard, K. Munch, E. Stephan,
894 M. Sablin, R. Sommer, T. Sipko, E. Scott, M. Suchard, A. Tikhonov, R. Willerslev,
895 R. Wayne, A. Cooper, M. Hofreiter, A. Sher, B. Shapiro, C. Rahbek, and E. Willerslev.
896 2011. Species-specific responses of Late Quaternary megafauna to climate and humans.
897 *Nature* 479:359–365.

898 Metropolis, N., A. Rosenbluth, M. Rosenbluth, A. Teller, and E. Teller. 1953. Equation of
899 state calculation by fast computing machines. *Journal of Chemical Physics* 21:1087–1092.
900

901 Minin, V., E. Bloomquist, and M. Suchard. 2008. Smooth skyride through a rough skyline:
902 Bayesian coalescent based inference of population dynamics. *Molecular Biology and*
903 *Evolution* 25:1459–1471.

904 Notohara, M. 1990. The coalescent and the genealogical process in geographically
905 structured population. *Journal of Mathematical Biology* 29:59–75.

906 Opgen-Rhein, R., L. Fahrmeir, and K. Strimmer. 2005. Inference of demographic history
907 from genealogical trees using reversible jump Markov chain Monte Carlo. *BMC*
908 *Evolutionary Biology* 5:6.

909 Palacios, J. and V. Minin. 2013. Gaussian process-based Bayesian nonparametric inference
910 of population size trajectories from gene genealogies. *Biometrics* 69:8–18.

911 Palstra, F. and D. Fraser. 2012. Effective/census population size ratio estimation: a
912 compendium and appraisal. *Ecology and Evolution* 2:2357–2365.

913 Powell, R., D. Barengolts, L. Mayr, and P. Nyambi. 2010. The evolution of HIV-1 diversity
914 in rural Cameroon and its implications in vaccine design and trials. *Viruses* 2:639–654.

915 Pybus, O., A. Rambaut, and P. Harvey. 2000. An integrated framework for the inference of
916 viral population history from reconstructed genealogies. *Genetics* 155:1429–1437.

917 Rodrigo, A. and J. Felsenstein. 1999. Coalescent Approaches to HIV Population Genetics
918 Pages 233–274. Johns Hopkins University Press, Baltimore, MD.

919 Shapiro, B., A. Drummond, A. Rambaut, M. Wilson, P. Matheus, A. Sher, O. Pybus,
920 M. Gilbert, I. Barnes, J. Binladen, E. Willerslev, A. Hansen, G. Baryshnikov, J. Burns,
921 S. Davydov, J. Driver, D. Froese, C. Harington, G. Keddie, P. Kosintsev, M. Kunz,
922 L. Martin, R. Stephenson, J. Storer, R. Tedford, S. Zimov, and A. Cooper. 2004. Rise
923 and fall of the Beringian steppe bison. *Science* 306:1561–1565.

924 Slatkin, M. and R. Hudson. 1991. Pairwise comparison of mitochondrial DNA sequences in
925 stable and exponentially growing populations. *Genetics* 129:555–562.

926 Stiller, M., G. Baryshnikov, H. Bocherens, A. Grandal-d’Anglade, B. Hilpert, S. Munzel,
927 R. Pinhasi, G. Rabeder, W. Rosendahl, E. Trinkaus, M. Hofreiter, and M. Knapp. 2010.
928 Withering away-25,000 years of genetic decline preceded cave bear extinction. *Molecular*
929 *Biology and Evolution* 27:975–978.

930 Strimmer, K. and O. Pybus. 2001. Exploring the demographic history of DNA sequences
931 using the generalized skyline plot. *Molecular Biology and Evolution* 18:2298–2305.

- 932 Stuart, A., P. Kosintsev, T. Higham, and A. Lister. 2004. Pleistocene to Holocene
933 extinction dynamics in giant deer and woolly mammoth. *Nature* 431:684–689.
- 934 Suchard, M., C. Kitchen, J. Sinsheimer, and R. Weiss. 2003. Hierarchical phylogenetic
935 models for analyzing multipartite sequence data. *Systematic Biology* 52:649–664.
- 936 Tener, J. 1965. Muskoxen in Canada: a biological and taxonomic review. Wildlife Service
937 Monograph Series No. 2 .
- 938 UNAIDS. 2015. AIDSinfo. <http://aidsinfo.unaids.org/>.
- 939 Volz, E., S. K. Pond, M. Ward, A. L. Brown, and S. Frost. 2009. Phylodynamics of
940 infectious disease epidemics. *Genetics* 183:1421–1430.
- 941 WHO. 2015a. World Health Organization, Dengue.
942 <http://www.who.int/topics/dengue/en/>.
- 943 WHO. 2015b. World Health Organization, Rabies. <http://www.who.int/rabies/en/>.
- 944 Wright, S. 1931. Evolution in Mendelian populations. *Genetics* 16:97–159.